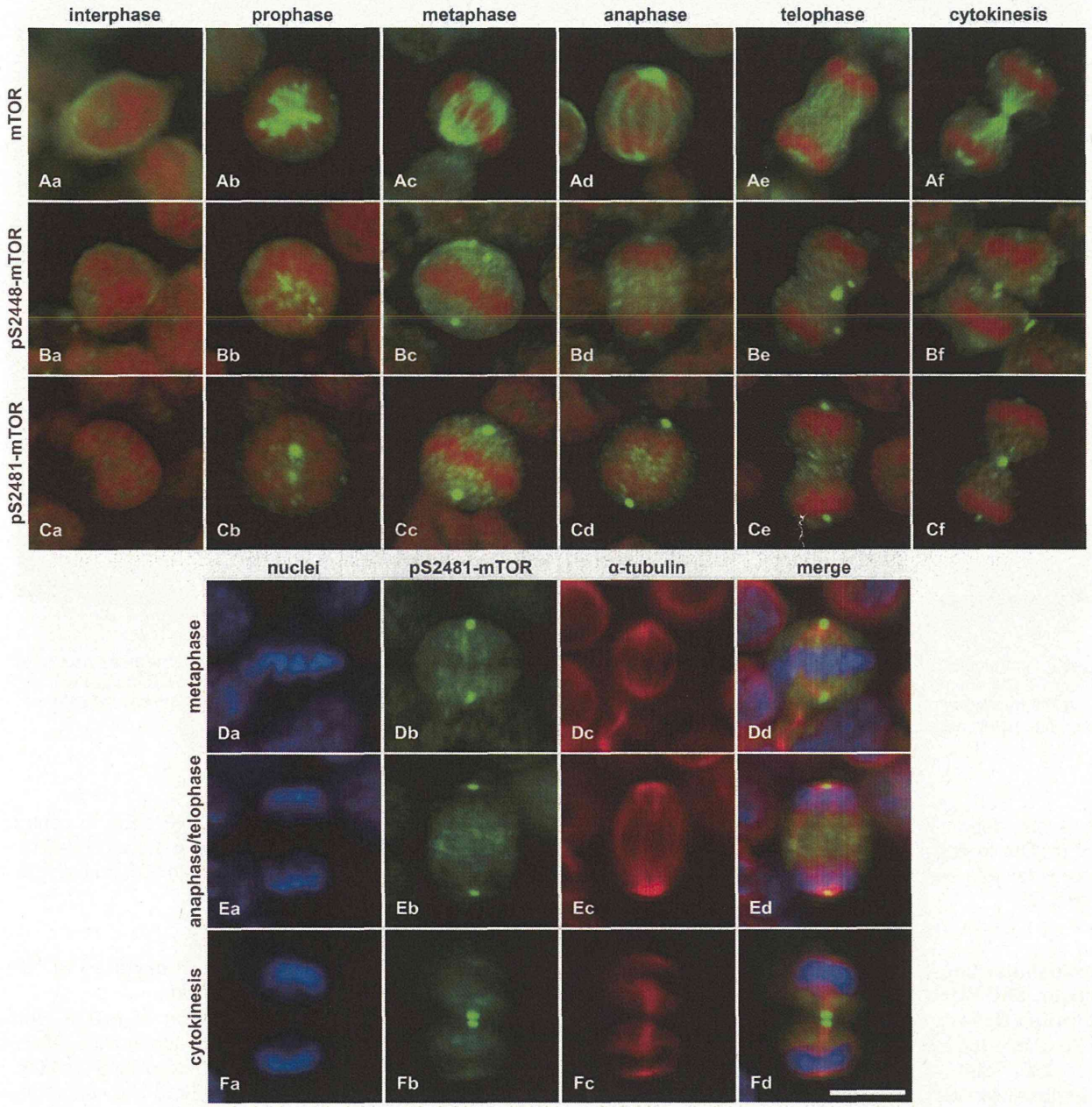

Figure 2. Intracellular localization of mTOR and phosphorylated mTOR at each stage of mitosis in mouse cumulus cells. Panels **Aa–Cf** show mTOR (**Aa–Af**), pS2448-mTOR (**Ba–Bf**), and pS2481-mTOR (**Ca–Cf**) staining, and contain one interphase cell image and five mitotic-phase cell images classified by nuclear status: interphase (**Aa**, **Ba**, **Ca**), prophase (**Ab**, **Bb**, **Cb**), metaphase (**Ac**, **Bc**, **Cc**), anaphase (**Ad**, **Bd**, **Cd**), telophase (**Ae**, **Be**, **Ce**), and cytokinesis (**Af**, **Bf**, **Cf**). Red and green represent nuclei and mTOR/p-mTOR, respectively. Panels **Da–Fd** show nuclei (**Da**, **Ea**, **Fa**), pS2481-mTOR (**Db**, **Eb**, **Fb**), α-tubulin (**Dc**, **Ec**, **Fc**), and merged images (**Dd**, **Ed**, **Fd**), and contain three step-wise mitotic-phase cells including the spindle in metaphase (**Da–Dd**), anaphase/telophase (**Ea–Ed**), and cytokinesis (**Fa–Fd**). Red, green, and blue represent α-tubulin, pS2481-mTOR, and nuclei, respectively. Scale bar, 10 μm.

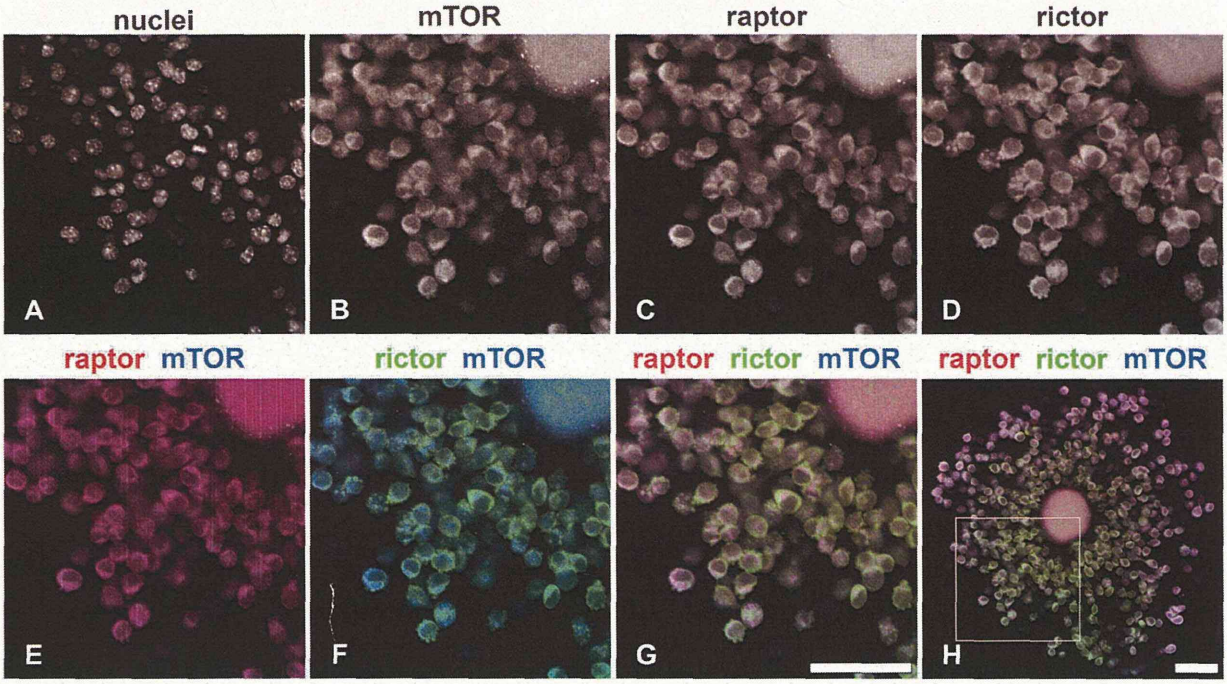

Figure 3. Immunolocalization of mTOR, raptor, and rictor in mouse cumulus cells. The panels show enlarged images of the area surrounded by squares (**A–G**) from the whole cumulus-oocyte complexes (**H**), including nuclei (**A**), mTOR (**B**), raptor (**C**), rictor (**D**), mTOR merged with raptor (**E**), mTOR merged with rictor (**F**), and mTOR merged with raptor and rictor (**G**, **H**). In the merged images, blue, red, and green represent mTOR, raptor, and rictor, respectively. Scale bars, 50 μm.

could not determine definitively whether or not rictor and mTOR exhibited colocalization. In some interphase cells, rictor was dispersed in a punctate pattern (Fig. 3D, F, and G).

Intracellular Localization Dynamics of mTOR, Raptor, and Rictor During Mitosis in Mouse Cumulus Cells

To clarify the distribution and colocalization of raptor and rictor with mTOR during mitosis, we analyzed the subcellular immunolocalization of mTOR, raptor, and rictor during the series of mitotic steps in cumulus cells by the triple staining procedure. Figure 4Ba–Df shows the individual distributions of mTOR, raptor, and rictor, and Figure 4Ea–Gf shows the colocalization of these proteins. Both raptor and rictor were expressed in the cytoplasm at all stages, and subtly in the nucleus at interphase (Fig. 4Ca–Df). Localization of raptor changed during mitotic progression: raptor was distributed in the cytoplasm and the nucleus at interphase (Fig. 4Ca), but was localized predominantly around the chromosomes at prophase (Fig. 4Cb) and on the spindle between metaphase and cytokinesis (Fig. 4Cc–Cf). Additionally, raptor colocalized with mTOR in the cytoplasm and the nucleus at interphase, around the chromosomes at prophase, and on the spindle from metaphase to cytokinesis (Fig. 4Ea–Ef). In contrast, cytoplasmic rictor was localized around, but excluded from, the spindle and did not colocalize with mTOR during mitosis (Fig. 4Da–Df and Fa–Ff).

Distribution of mTOR and Phosphorylated mTOR During Mouse Oocyte Maturation

We next assessed the distribution of mTOR during meiotic maturation using immunofluorescence staining to detect mTOR, pS2448-mTOR, and pS2481-mTOR in mouse oocytes. Oocytes in non-cultured GV, cultured GV, GVBD, MI, anaphase I (AI)/telphase I (TI), and MII stages were, respectively, collected at 0, 4, 6, 10, 12, and 18 hr after culture. The expression of mTOR, pS2448-mTOR, and pS2481-mTOR was confirmed in the cytoplasm at every stage of meiotic maturation (Fig. 5A–U). mTOR was observed exclusively in the cytoplasm in non-cultured GV oocytes (Fig. 5A), but displayed a punctate pattern in the nucleus in cultured GV oocytes (Fig. 5B), intense localization around the chromosomes at GVBD (Fig. 5C), and localization on the spindle during MI–MII stages (Fig. 5D–G). Both pS2448-mTOR and pS2481-mTOR were distributed in a punctate manner in the cytoplasm and nucleus at the non-cultured GV stage (Fig. 5H and O). Meanwhile, they were detected uniformly in the cytoplasm

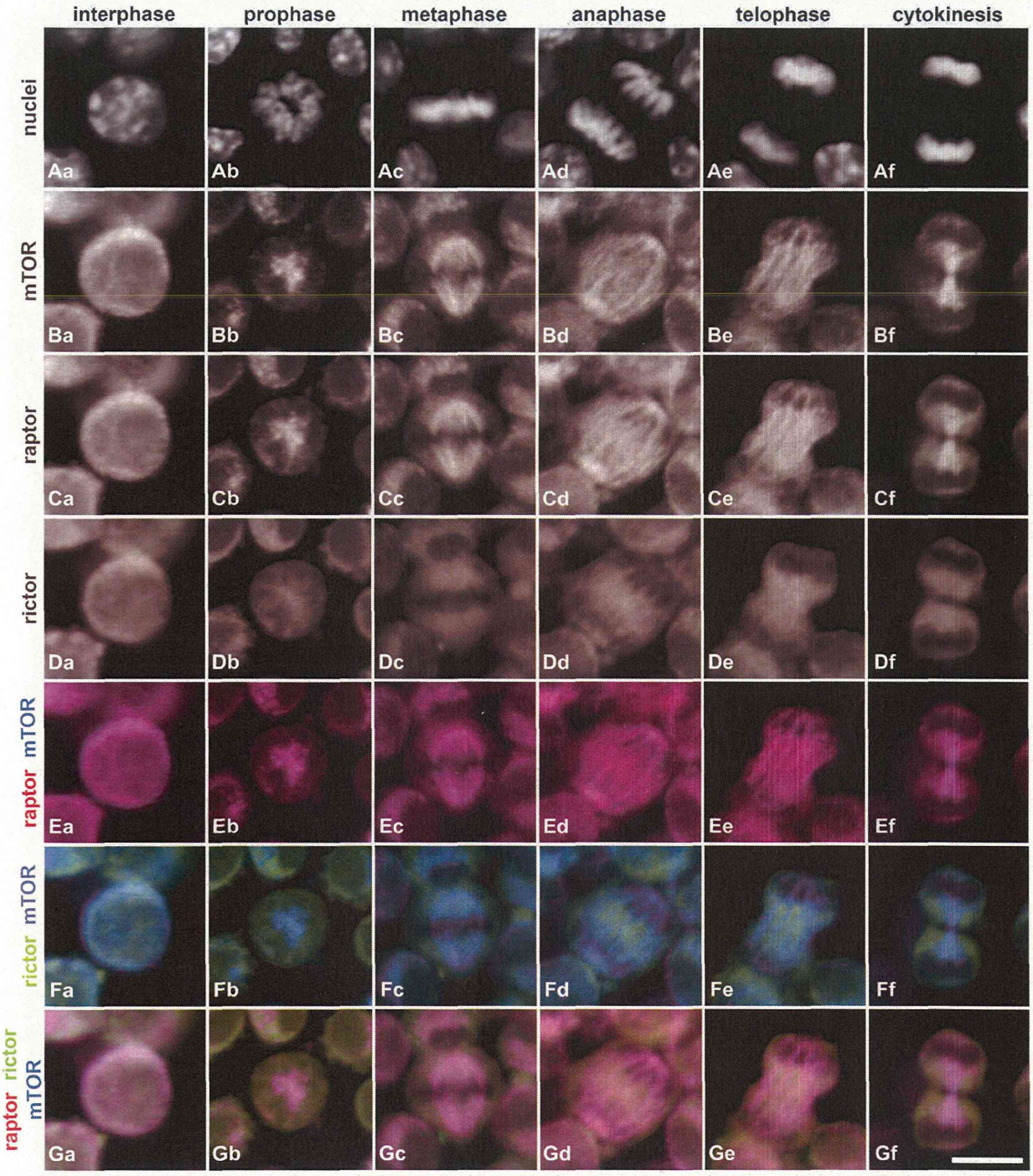

Figure 4. Intracellular localization of mTOR, raptor, and rictor at each stage of mitosis in mouse cumulus cells. The panels show nuclei (**Aa–Af**), mTOR (**Ba–Bf**), raptor (**Ca–Cf**), rictor (**Da–Df**), mTOR merged with raptor (**Ea–Ef**), mTOR merged with rictor (**Fa–Ff**), and mTOR merged with raptor and rictor (**Ga–Gf**), containing one interphase cell image and five mitotic-phase cell images classified by nuclear status: interphase (**Aa**, **Ba**, **Ca**, **Da**, **Ea**, **Fa**, **Ga**), prophase (**Ab**, **Bb**, **Cb**, **Db**, **Eb**, **Fb**, **Gb**), metaphase (**Ac**, **Bc**, **Cc**, **Dc**, **Ec**, **Fc**, **Gc**), anaphase (**Ad**, **Bd**, **Cd**, **Dd**, **Ed**, **Fd**, **Gd**), telophase (**Ae**, **Be**, **Ce**, **De**, **Ee**, **Fe**, **Ge**), and cytokinesis (**Af**, **Bf**, **Cf**, **Df**, **Ef**, **Ff**, **Gf**). In panels **Ea–Gf**, red, green, and blue represent raptor, rictor, and mTOR, respectively. Scale bar, 10 μm.

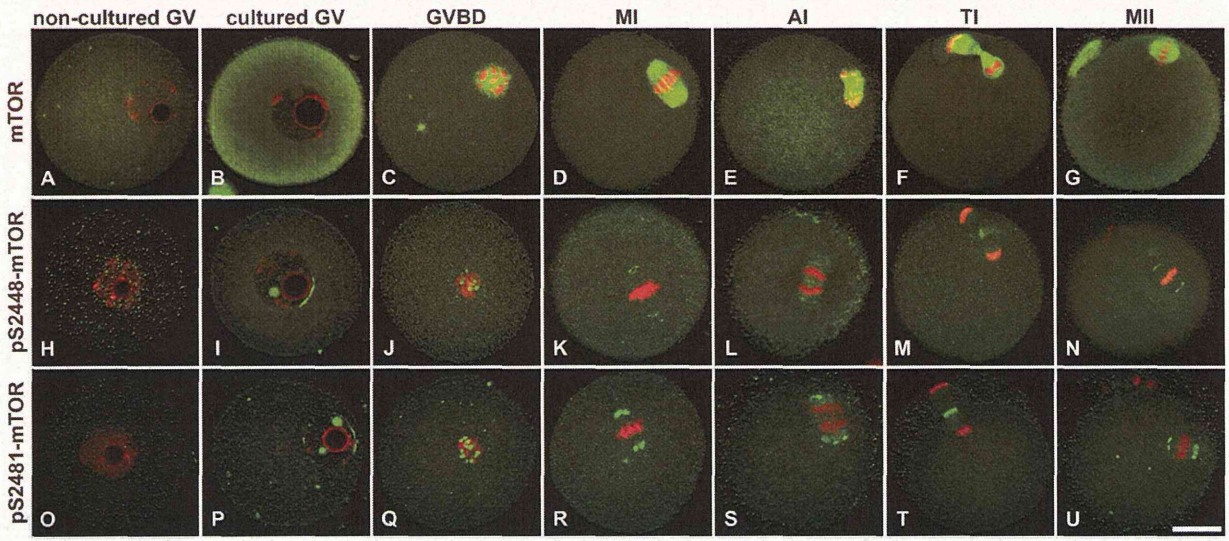

Figure 5. Intracellular localization of mTOR and phosphorylated mTOR during meiotic maturation in mouse oocytes. The panels show mTOR (**A–G**), pS2448-mTOR (**H–N**), and pS2481-mTOR (**O–U**), and contain seven step-wise images of oocyte maturation classified by nuclear status: non-cultured GV stage (0 hr; **A**, **H**, **O**), cultured GV stage (4 hr; **B**, **I**, **P**), GVBD (6 hr; **C**, **J**, **Q**), metaphase I (MI) (10 hr; **D**, **K**, **R**), anaphase I (AI) (12 hr; **E**, **L**, **S**), telophase I (TI) (12 hr; **F**, **M**, **T**), and metaphase II (MII) (18 hr; **G**, **N**, **U**). Red and green represent nuclei and mTOR/p-mTOR, respectively. Scale bar, 20 μm.

and exhibited robust localization after the non-cultured GV stage (Fig. 5I–N and P–U). Both forms of phosphorylated mTOR were localized at the nuclear envelope and inner nucleus in a punctate manner at the non-cultured GV stage (Fig. 5I and P), in the vicinity of the chromosomes as multiple dots at GVBD (Fig. 5J and Q), on the spindle poles at MI/AI/MII (Fig. 5K, L, N, R, S, and U), and on the midbodies at TI (Fig. 5M and T). Both forms of phosphorylated mTOR colocalized with pericentrin, located near part of the nuclear envelope at the cultured GV stage (Fig. 6Aa–Ad and Ea–Ed), around the chromosomes at GVBD (Fig. 6Ba–Bd and Fa–Fd), and on the spindle poles of MI/MII oocytes (Fig. 6Ca–Dd and Ga–Hd). Colocalization was also observed as overlapping tiny dots in the cytoplasm of several oocytes stages (Fig. 6Aa–Hd).

Ooplasmic Fluorescence Intensity of Phosphorylated mTOR was Elevated With the Re-Initiation of Meiosis

Both forms of phosphorylated mTOR were strongly expressed in mitotic cumulus cells (Fig. 1). To investigate changes in the phosphorylation dynamics of mTOR during oocyte maturation, we compared the fluorescence intensities of the two phosphorylated forms of mTOR in non-cultured GV oocytes (before meiotic resumption), cultured GV oocytes (just before meiotic resumption), at GVBD (onset of meiotic maturation), and at MII (endpoint of meiotic maturation). The perivitelline space is known to be formed at the GV stage, just before GVBD (Inoue et al., 2007). Therefore, from the same preparation, we discriminated non-cultured GV from cultured GV oocytes by the existence of the perivitelline space, and GVBD from MII by the existence of the first polar body (Fig. 7A and D). Fluorescence intensity was compared using fluorescence (Fig. 7B and E) and pseudo-color images (Fig. 7C and F). Both pS2448-mTOR and pS2481-mTOR displayed stronger intensities in cultured GV oocytes than in non-cultured GV oocytes, and stronger intensity was also observed at GVBD/MII than at the cultured GV stage (Fig. 7B, C, E, and F). In addition, the average fluorescence intensity per unit area in the cytoplasmic intensities of both pS2448-mTOR and pS2481-mTOR were significantly higher at the cultured GV than at non-cultured GV stage, and significantly increased during the transition from non-cultured GV to GVBD stages (Fig. 7G and H). Significant differences in elevated intensities were only observed for pS2448-mTOR, despite parallel increases between GVBD and MII for both phosphorylated forms. These results suggested that mTOR was dramatically phosphorylated over the course of meiotic resumption.

Distribution of mTOR, Raptor, and Rictor During Mouse Oocyte Maturation

To validate the subcellular localization of raptor and rictor with mTOR at different stages of oocyte maturation, triple staining was performed. Raptor expression was observed in the cytoplasm at all stages (Fig. 8Ca–Cg). While raptor was distributed throughout the cytoplasm at the non-cultured GV stage (Fig. 8Ca), it exhibited punctate

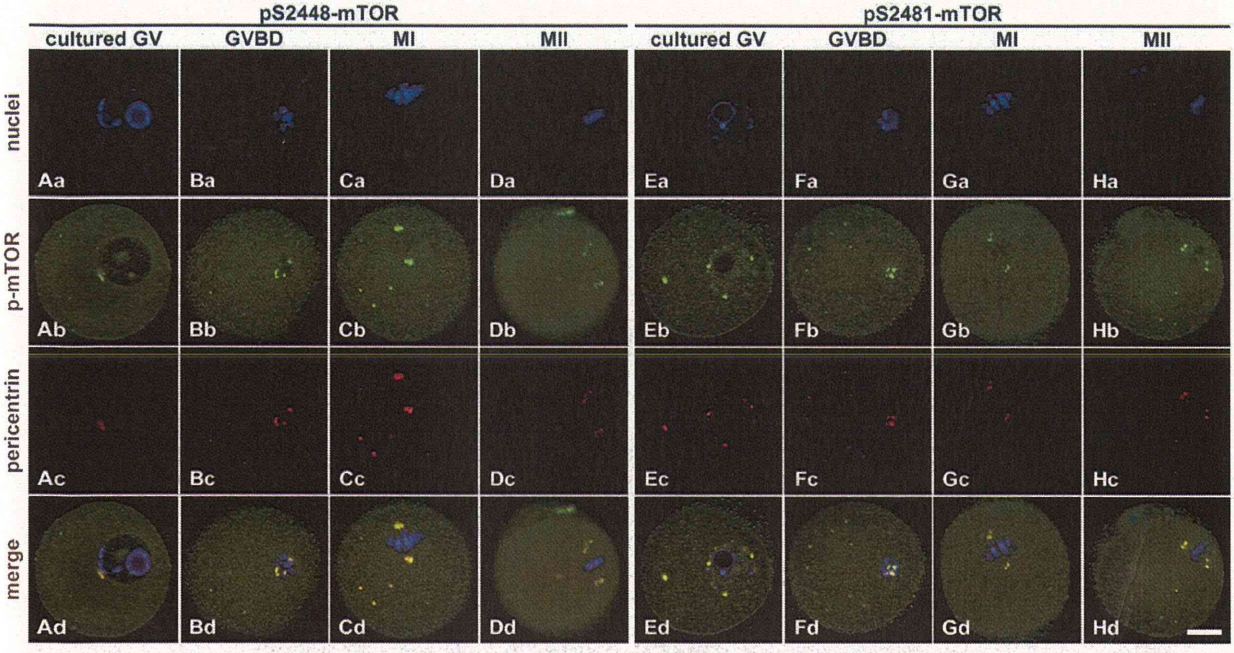

Figure 6. Intracellular localization of phoshorylated mTOR and pericentrin during meiotic maturation in mouse oocytes. The panels show nuclei (**Aa**, **Ba**, **Ca**, **Da**, **Ea**, **Fa**, **Ga**, **Ha**), phoshorylated mTOR (**Ab**, **Bb**, **Cb**, **Db**, **Eb**, **Fb**, **Gb**, **Hb**), pericentrin (**Ac**, **Bc**, **Cc**, **Dc**, **Ec**, **Fc**, **Gc**, **Hc**), and merged images (**Ad**, **Bd**, **Cd**, **Dd**, **Ed**, **Fd**, **Gd**, **Hd**), containing four step-wise images of oocytes undergoing meiotic maturation with phosphorylated mTOR showed analogous localization with MTOCs: cultured GV (4 hr, **Aa–Ad**, **Ea–Ed**), GVBD (6 hr, **Ba–Bd**, **Fa–Fd**), MI (10 hr, **Ca–Cd**, **Ga–Gd**), and MII (18 hr, **Da–Dd**, **Ha–Hd**). Red, green, and blue represent pericentrin, phosphorylated mTOR, and nuclei, respectively. Scale bar, 20 μm.

localization in the GV in cultured GV oocyts (Fig. 8Cb). Raptor later accumulated around the chromosomes at GVBD (Fig. 8Cc), and localized on the spindle from MI to MII stages (Fig. 8Cd–Cg). Moreover, raptor colocalized with mTOR in a punctate pattern in the nucleus, around the chromosomes, and on the spindle at the cultured GV stage, GVBD, and MI–MII stages, respectively (Fig. 8Ea–Eg). In contrast, rictor exhibited a spongiform pattern in the cytoplasm during meiotic maturation (Fig. 8Da–Dg). Rictor was distributed exclusively in the cytoplasm at the non-cultured GV stage, GVBD, and AI–MII stages (Fig. 8Da, Dc, and De–Dg), but localized in the nucleus in a punctate pattern at the cultured GV stage (Fig. 8Db) and around the spindle poles at the MI stage (Fig. 8Dd). The colocalization of rictor and mTOR was not observed in the cytoplasm (Fig. 8Fa–Fg). As shown in Figure 8Fd and Gd, rictor accumulated not only on the pole area of spindle but also in the cytoplasm close to the spindle poles.

DISCUSSION

In the present study, we analyzed the distribution of mTOR, phosphorylated mTOR, and representative cofactors of the two mTOR complexes, raptor and rictor, in mouse cumulus cells and oocyte in order to estimate the roles of each mTOR complex during oocyte maturation and to compare the results with those observed during mitosis. We demonstrated that mTOR, phosphorylated mTOR, and raptor share similar distribution associated with the spindle apparatus in two cell division systems, while rictor markedly localized around the first meiotic spindle poles.

mTOR is activated by phosphorylation of several amino acid residues; phosphorylation at Ser2448 and Ser2481 is recognized as a marker of intrinsic mTOR catalytic activity (Altomare et al., 2004; Lawrence et al., 2004; Yonezawa et al., 2004). Thus, we first examined the distribution of Ser2448- and Ser2481-phosphorylated mTOR in addition to total mTOR. During mitosis in mouse cumulus cells, while accumulation of mTOR was observed around the chromosomes and on the spindle, phosphorylated mTOR was highly expressed in mitotic cells and displayed punctate localization adjacent to the chromosomes, on the spindle poles and the midbody. These expression patterns were consistent with previous studies in somatic cells demonstrating that pS2448- and pS2481-mTOR localized on the spindle poles and the midbody in mouse granulosa cells and several types of cancer cells (Yaba et al., 2008; Vazquez-Martin et al., 2009a, 2012; Doghman et al., 2010; Lopez-Bonet et al., 2010). These data, therefore, suggest that mTOR is involved in mitotic and cytokinetic spindle function, particularly through the regulation of centrosomes by the

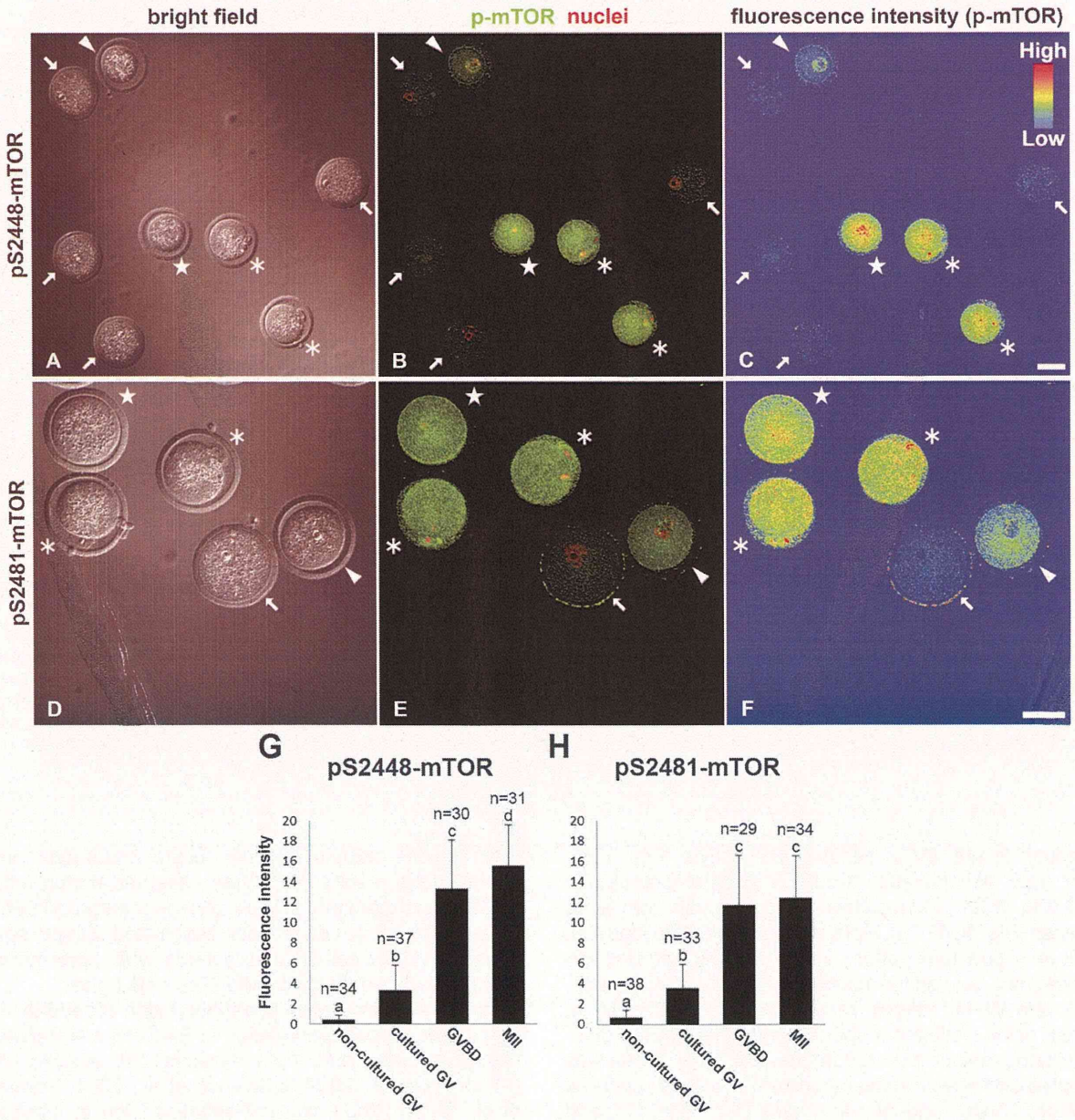

Figure 7. Comparison of fluorescence intensity for phosphorylated mTOR in the cytoplasm during meiotic resumption in mouse oocytes. The panels show pS2448-mTOR (**A–C**) and pS2481-mTOR (**D–F**). Panels **A** and **D**, **B** and **E**, and **C** and **F** represent brightfield, nuclei/p-mTOR, and pseudo-color images, respectively, and represent differences in fluorescence intensities. The arrow, arrowhead, star, and asterisk represent non-cultured GV, cultured GV, GVBD, and MII stages, respectively. Scale bar, 20 μm. The bar charts show quantified fluorescence ratios for pS2448-mTOR (**G**) and pS2481-mTOR (**H**). The total number of oocytes analyzed (n) for each meiotic stage is indicated at the top of the columns. Values are expressed as means ± standard deviation. Bars with different superscripts (a–d) are significantly different ($P < 0.05$).

activated form of mTOR. Furthermore, the fact that mTOR exclusively colocalized with raptor around the chromosomes and on the spindle during cumulus cell mitosis supports that, of the two mTOR complexes, mTORC1 was predominantly associated with mitotic events. Raptor has various phosphorylation sites that appear to be critical to the regulation of mTORC1 activity (Wang et al., 2009; Foster et al., 2010). Moreover, seven phosphorylation sites (i.e., Ser696, Thr706, Ser722, Ser855, Ser859, Ser863, and Ser877) were hyperactive in mitosis and involved in

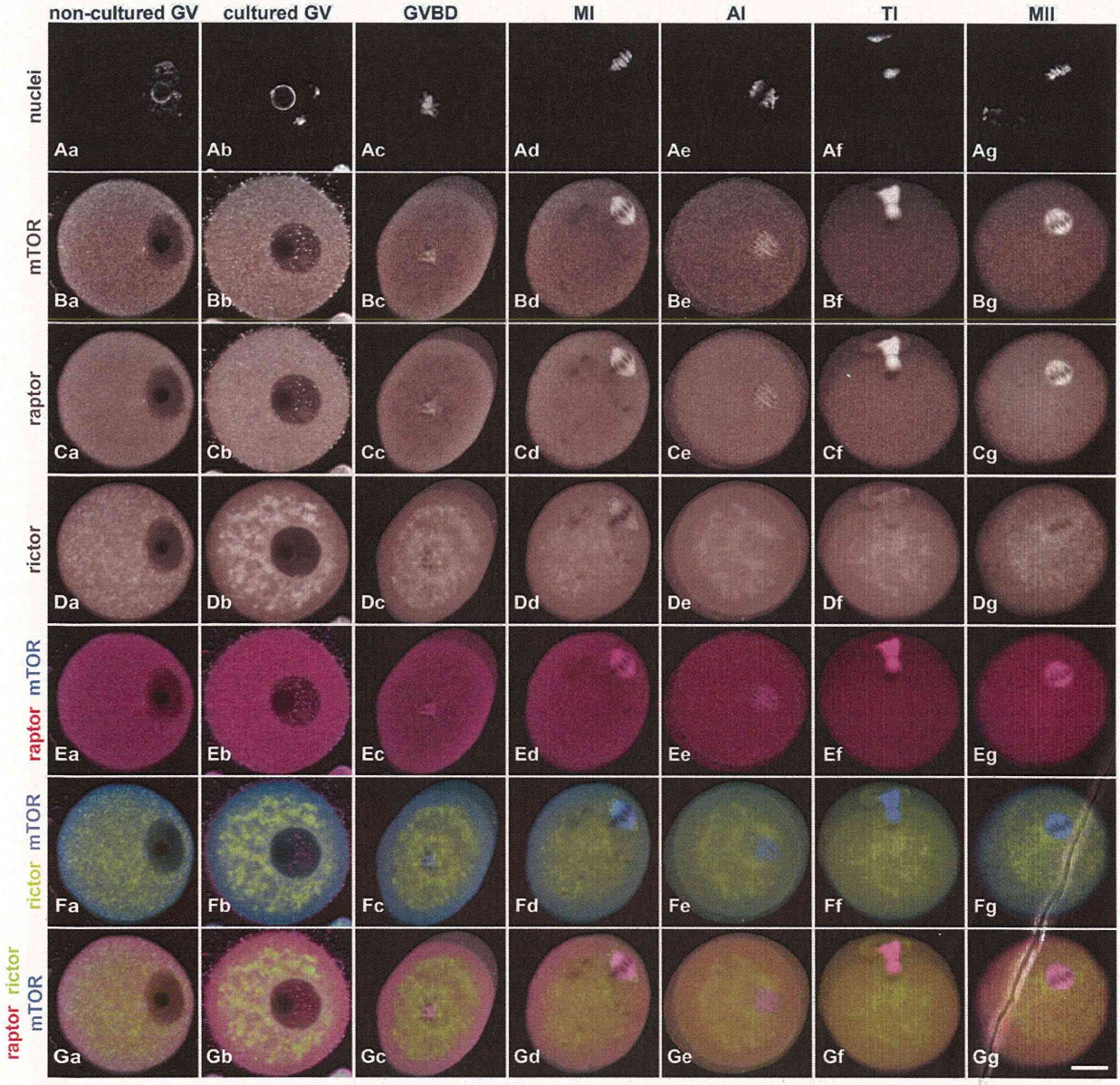

Figure 8. Intracellular localization of mTOR, raptor, and rictor during meiotic maturation in mouse oocytes. The panels show nuclei (**Aa–Ag**), mTOR (**Ba–Bg**), raptor (**Ca–Cg**), rictor (**Da–Dg**), mTOR merged with raptor (**Ea–Ef**), mTOR merged with rictor (**Fa–Ff**), and mTOR merged with raptor and rictor (**Ga–Gf**), containing seven step-wise images of oocyte maturation classified by nuclear status: non-cultured GV stage (0 hr; **Aa**, **Ba**, **Ca**, **Da**, **Ea**, **Fa**, **Ga**), cultured GV stage (4 hr; **Ab**, **Bb**, **Cb**, **Db**, **Eb**, **Fb**, **Gb**), GVBD (6 hr; **Ac**, **Bc**, **Cc**, **Dc**, **Ec**, **Fc**, **Gc**), metaphase I (MI) (10 hr; **Ad**, **Bd**, **Cd**, **Dd**, **Ed**, **Fd**, **Gd**), anaphase I (AI) (12 hr; **Ae**, **Be**, **Ce**, **De**, **Ee**, **Fe**, **Ge**), telphase I (TI) (12 hr; **Af**, **Bf**, **Cf**, **Df**, **Ef**, **Ff**, **Gf**), and metaphase II (MII) (18 hr; **Ag**, **Bg**, **Cg**, **Dg**, **Eg**, **Fg**, **Gg**). In panels **Ea–Gg**, red, green, and blue represent raptor, rictor, and mTOR, respectively. Scale bar, 20 μm.

mitosis-regulated protein kinase signaling to facilitate cell-cycle progression through the G_2/M phase (Gwinn et al., 2010; Ramirez-Valle et al., 2010). Recently, another investigation revealed that while both Ser722- and Ser877-phosphorylated raptor are located at the centrosomal region, Thr706- and Ser863-phosphorylated raptor are found in loci of the midbody during mitosis (Vazquez-Martin et al., 2011). Similar expression has also been observed in components of the mTORC1 pathway, such as the upstream regulators PI3K, Akt, TSC1/2, AMPK, and MAPK, as well as the downstream effectors S6K2 and 4E-BP1, which are hyperactive in the mitotic phase and localize on the spindle,

mitotic centrioles, and midbody loci (Kapeller et al., 1995; Wakefield et al., 2003; Delaval et al., 2005; Cha et al., 2007; Gui et al., 2007; Rossi et al., 2007; Vazquez-Martin et al., 2009b; Gomez-Baldo et al., 2010; Yu et al., 2011). These data support the possibility that mTORC1 participates in spindle function and suggest that raptor phosphorylation and mTORC1 signaling are involved in this machinery.

During oocyte meiotic maturation in mice, while mTOR and raptor also colocalized around the chromosomes and on the spindle, the immunofluorescence intensity of phosphorylated mTOR increased during meiotic resumption and displayed a speckled localization pattern adjacent to the chromosomes, on the spindle poles, and on the midbody. It has also been reported that Akt, AMPK, and MAPK exhibit dynamic distribution during meiosis: these proteins are dramatically phosphorylated around GVBD and localized on the meiotic spindle, at sites similar to mTOR during mouse meiotic maturation (Verlhac et al., 1993; Hoshino et al., 2004; Kalous et al., 2006; Hoshino and Sato, 2008; Downs et al., 2010). These localization patterns, similar to those observed during mitosis, reflect the functional analog of mTORC1 for the meiotic spindle during oocyte maturation.

Coupled with expression status, evidence is building for mitotic-phase-specific roles for mTORC1 signaling. mTOR interacts directly with and phosphorylates clip-170, a microtubule-associated protein (MAP); moreover, mTOR regulates the function of clip-170, stabilizing the microtubule fiber structures and spindle morphology in yeast and human cells (Choi et al., 2000, 2002). During cell division, clip-170 is known to be located on the spindle, similar to mTOR (Rickard and Kreis, 1990; Dujardin et al., 1998; Brunet et al., 1999). Biochemical studies have found that treatment with rapamycin, a preferential mTORC1 inhibitor, leads to chromosomal nondisjunction during mitotic-phase in yeast and mammalian cell cultures (Bonatti et al., 1998, 2005; Yu et al., 2012). Genetic studies, such as knockdown of TSC1/2, the negative upstream regulator of mTORC1, have shown that impairment of spindle formation caused by excessive centrosome amplification and polyploidy can result from over-activation of mTORC1; this phenotype was recovered by treatment with rapamycin in cancer cells (Astrinidis et al., 2006). Our results support these same roles for mTORC1 during oocyte meiosis that is modulation of meiotic microtubule stabilization, centrosome-dependent spindle formation, and chromosome segregation. Typical oocytes lack centrosomes, however, and instead use acentriolar MTOCs that substitute as centrosomes during acentrosomal spindle assembly (Manandhar et al., 2005). Before GVBD, MTOCs are distributed throughout the cytoplasm and aggregate into a portion of the nuclear periphery of mouse oocytes, push against the nuclear envelope, and cause invaginations, presumably resulting in tearing of the nuclear membranes and facilitating the transition into GVBD. After GVBD, MTOCs recruit chromosomes and form the spindle (Beaudouin et al., 2002; Schuh and Ellenberg, 2007). We demonstrated that phosphorylated mTOR colocalized with MTOCs: positioning in perinuclear regions in cultured GV oocytes, around the chromosomes at GVBD, and on the spindle poles at MI and MII stages. Rapamycin has been shown to suppress the emergence of GVBD in mouse oocytes (Yan-Chang and Cai-Rong, 2009). Hence, we assume that mTOR is involved in MTOC-dependent meiotic resumption and acentrosomal spindle formation.

We also observed that rictor exhibited a differential distribution pattern between mitosis in cumulus cells and oocyte maturation. Rictor was expressed in the cytoplasm during mitosis, but localized to the nucleus, forming a punctate pattern, in cultured GV oocytes and around the spindle poles at the MI stage during meiotic maturation.

Oocyte meiotic divisions are extremely asymmetric, giving rise to a large oocyte and small degenerating polar bodies, while retaining the maternal stores for further embryo development. This asymmetry is achieved by off-center positioning of the division spindle (Gonczy, 2008). Though the MII spindle is originally formed near the cortex without migration, the MI spindle is generated in the center of the cytoplasm and is then transported to the cell cortex (Verlhac et al., 2000). Due to the absence of centrioles and astral microtubules, spindle translocation depends on the cytoplasmic meshwork of F-actin filaments (Longo and Chen, 1985). During spindle migration in mouse oocytes, actin filaments progressively organize into a "spindle-like" structure; most of the filaments form along the microtubules, obviously present inside the spindle. Actin filaments also expand from spindle poles to closed areas in the cytoplasm, connecting to the cortex when they are finished migrating (Azoury et al., 2008, 2011). At the MI stage, considered the midpoint of migration, localization of rictor was clearly consistent with the proposed actin dynamics and with the role of mTORC2 in regulating organization of the actin cytoskeleton (Jacinto et al., 2004; Sarbassov et al., 2004). Injection of mouse oocytes with anti-mTOR antibodies has been shown to cause failure of peripheral spindle migration and asymmetric division (Lee et al., 2012). Although, we were not able to determine the precise colocalization of mTOR and rictor around the meiotic spindle, it seems that mTORC2 may be involved in actin organization-dependent spindle migration during oocyte maturation.

In cultured GV oocytes, mTOR, phosphorylated mTOR, raptor, and rictor showed punctate localization in the nucleus. This suggests that both mTOR complexes function in the nucleus. Nevertheless, we did not observe these localization patterns at non-cultured GV stages, suggesting that these complexes have significant roles in the onset of GVBD.

Another speculation is that mTOR is involved in the development of fertilizable oocytes through cumulus cell proliferation. In expanded, peri-ovulatory cumulus-oocyte complexes (COCs), almost all cumulus cells are in the G_0/G_1 phase of the cell cycle (Schuetz et al., 1996). During meiotic maturation, cumulus cells are thought to undergo terminal differentiation, represented by broad changes in gene expression profiles and mucification, for example the production of extracellular matrix components, and are generally not assumed to be mitotic. Recently, however,

in vivo injection of human chronic gonadotropin (hCG) has been shown to transiently upregulate the proliferative activity of cumulus cells in concert with early meiotic division in mice (Hernandez-Gonzalez et al., 2006). Although current research has not investigated proliferation ratios, we observed mitotic cumulus cells in our in vitro maturation system, supporting previous investigations. Furthermore, the number of cumulus cells is positively correlated with the developmental competence of oocytes (Leibfried-Rutledge et al., 1989; Hashimoto et al., 1998). Ovulatory input to mural granulosa cells is mediated by cumulus cells via paracrine signaling and cell-to-cell interactions (Conti et al., 2006), and cumulus cells directly produce and secrete a diffusible meiosis-inducing substances, named follicular fluid-meiosis activating sterol (Byskov et al., 1995). Thus, the proliferative activity of cumulus cells in the meiotic maturation phase is considered to be essential for the generation of oocytes with sufficient developmental capacity. Phosphorylated mTOR was highly condensed in mitotic cumulus cells, thus mTOR may also contribute to the production of developmentally high-grade oocytes via promotion of cumulus cell proliferation.

Taken together, our data suggested the possibility that mTORC1 is involved in the regulation of spindle assembly and functions in both cumulus cell mitosis and oocyte meiosis. In contrast, mTORC2 appeared to control asymmetric division via actin cytoskeleton-dependent spindle migration principally during meiotic maturation. Therefore, our data demonstrated that mTOR was involved in meiotic maturation directly and indirectly through regulation of the proliferative activity of cumulus cells in mouse oocytes.

MATERIALS AND METHODS

Animals

ICR mice were purchased from Japan SLC, Inc. (Shizuoka, Japan) and were bred in our laboratory. Immature 20- to 23-day-old female mice were used for all experiments. All studies were conducted according to the Guide for the Care and Use of Laboratory Animals published by Tohoku University.

Oocyte Collection and Culture

In vitro oocyte maturation was achieved according to previously described methods (Hoshino and Sato, 2008). Follicle development was stimulated by intraperitoneal injection with 5 IU of pregnant mare's serum gonadotropin (PMSG; Teikoku Hormone MFG, Tokyo, Japan). Cumulus-oocyte complexes (COCs) were isolated from mice 48 hr after PMSG injection by puncturing the large antral follicles with a 26-gauge needle, and were collected in Leibovitz's L-15 medium (Invitrogen, Grand Island, NY) containing 0.1% polyvinyl alcohol (PVA; Sigma, St. Louis, MO) and 4 mM hypoxanthine (Sigma) in order to maintain the oocytes at the GV stage. Collected COCs were cultured in Waymouth's MB752/1 medium (Invitrogen) containing 5% fetal calf serum (Sankyo Kagaku, Tokyo, Japan), 0.23 mM pyruvic acid (Nacalai Tesque, Kyoto, Japan), 75 mg/L penicillin G (Meiji Seika, Tokyo, Japan), 50 mg/L streptomycin sulfate (Meiji Seika), 4 mM hypoxanthine, and 100 IU/L FSH (Sigma). A total of 20–25 COCs were cultured in 100 μl droplets of culture medium overlaid with paraffin liquid (Nacalai Tesque) in a humidified atmosphere of 5% CO_2 in air at 37°C. COCs for immunostaining of cumulus cells were acquired after 8 hr of culture. To obtain oocytes at non-cultured GV, cultured GV, GVBD, MI, AI-TI, and MII stages, oocytes were cultured for 0, 4, 6, 10, 12, and 18 hr, respectively. Denuded oocytes were acquired by pipetting in the presence of 0.1% hyaluronidase (Sigma), thereby mechanically remove cumulus cells.

Immunostaining of Cumulus Cells and Oocytes

Immunolocalization in COCs and oocytes was analyzed according to previously described methods (Hoshino and Sato, 2008). COCs and oocytes were fixed with 2% paraformaldehyde (Sigma) in Dulbecco's phosphate-buffered saline without magnesium or calcium (PBS[−]) containing 0.1% PVA and 0.2% TritonX-100 at room temperature for 60 min. For single staining to detect mTOR or phosphorylated mTOR, we used anti-mTOR, anti-Ser2448-phosphorylated mTOR, and anti-Ser2481-phosphorylated mTOR antibodies (Cell Signaling Technology, Inc., Danvers, MA; catalog numbers 2972, 2971, and 2974, respectively; 1:100 dilution) and Alexa Fluor 488-conjugated goat anti-rabbit IgG (Molecular Probes, Eugene, OR; 1:200 dilution). For double staining to detect phosphorylated mTOR with α-tubulin or pericentrin, we used anti-α-tubulin IgG (Sigma; catalog number T9026; 1:500 dilution) and anti-pericentrin IgG (BD Transduction Laboratories, San Diego, CA; catalog number 611814; 1:250 dilution), with Alexa Fluor 568-conjugated goat anti-mouse IgG (Molecular Probes; 1:200 dilution). For triple staining to detect mTOR, raptor, and rictor, we used the Zenon technique according to previously published methods (van Duijnhoven et al., 2005), with slight modifications. First, mTOR was detected by anti-mTOR primary antibodies and Alexa Fluor 647-conjugated donkey anti-rabbit IgG (Molecular Probes; 1:200 dilution). Next, raptor and rictor were detected by anti-raptor antibodies (Cell Signaling Technology, Inc.; catalog number 2280; 1:100 dilution) labeled with Zenon Alexa Fluor 568-conjugated rabbit IgG and anti-rictor antibodies (Cell Signaling Technology, Inc; catalog number 2114; 1:100 dilution) labeled with Zenon Alexa Fluor 488-conjugated rabbit IgG (Molecular Probes), respectively. Nuclei were labeled with 10 μg/ml propidium iodide (Sigma) or Hoechst 33342 (Sigma). Images were acquired using a Zeiss LSM700 confocal microscope.

Fluorescence Quantification

A system for the quantification of cytoplasm fluorescence ratios was developed to analyze fluorescence localization within oocytes according to the method of Freudzon et al. (2005). Each image was acquired by an identical and automated process on the microscope. Cytoplasmic

fluorescence level was determined by drawing a closed polygon on the plasma membrane and calculating the average intensity within the surrounding region using Image J (http://rsb.info.nih.gov/ij/index.html; National Institute of Health, Bethesda, MD), after subtracting autofluorescence levels.

Statistical Analysis

For the statistical analysis of more than two groups, we used analysis of variance (ANOVA) followed by a Bonferroni/Dunn test with STATVIEW software (Abacus Concepts, Inc., Berkeley, CA). All experiments were repeated more than four times with at least 10 COCs or oocytes. Data are represented as means ± standard deviation, and means were considered significantly different when *P*-values were less than 0.05.

ACKNOWLEDGMENTS

This work was supported by a grant from the Japan Society for the Promotion of Science to E. Sato (No. 24248047). This work was also supported in part by a Grant-in-Aid for Young Scientists (B) to Y. Hoshino (No. 21780250) from the Ministry of Education, Science, and Culture, Japan.

REFERENCES

Alessi DR, Pearce LR, Garcia-Martinez JM. 2009. New insights into mTOR signaling: mTORC2 and beyond. Sci Signal 2:pe27.

Altomare DA, Wang HQ, Skele KL, De Rienzo A, Klein-Szanto AJ, Godwin AK, Testa JR. 2004. AKT and mTOR phosphorylation is frequently detected in ovarian cancer and can be targeted to disrupt ovarian tumor cell growth. Oncogene 23:5853–5857.

Astrinidis A, Senapedis W, Henske EP. 2006. Hamartin, the tuberous sclerosis complex 1 gene product, interacts with polo-like kinase 1 in a phosphorylation-dependent manner. Hum Mol Genet 15:287–297.

Astrinidis A, Kim J, Kelly CM, Olofsson BA, Torabi B, Sorokina EM, Azizkhan-Clifford J. 2010. The transcription factor SP1 regulates centriole function and chromosomal stability through a functional interaction with the mammalian target of rapamycin/raptor complex. Genes Chromosomes Cancer 49:282–297.

Azoury J, Lee KW, Georget V, Rassinier P, Leader B, Verlhac MH. 2008. Spindle positioning in mouse oocytes relies on a dynamic meshwork of actin filaments. Curr Biol 18:1514–1519.

Azoury J, Lee KW, Georget V, Hikal P, Verlhac MH. 2011. Symmetry breaking in mouse oocytes requires transient F-actin meshwork destabilization. Development 138:2903–2908.

Beaudouin J, Gerlich D, Daigle N, Eils R, Ellenberg J. 2002. Nuclear envelope breakdown proceeds by microtubule-induced tearing of the lamina. Cell 108:83–96.

Bhaskar PT, Hay N. 2007. The two TORCs and Akt. Dev Cell 12:487–502.

Bonatti S, Simili M, Galli A, Bagnato P, Pigullo S, Schiestl RH, Abbondandolo A. 1998. Inhibition of the Mr 70,000 S6 kinase pathway by rapamycin results in chromosome malsegregation in yeast and mammalian cells. Chromosoma 107:498–506.

Bonatti S, Simili M, Benedetti PA, Morandi F, Menichini P, Del Carratore R, Barale R, Abbondandolo A. 2005. Altered centrosomes in ataxia-telangiectasia cells and rapamycin-treated Chinese hamster cells. Environ Mol Mutagen 46:164–173.

Brunet S, Maria AS, Guillaud P, Dujardin D, Kubiak JZ, Maro B. 1999. Kinetochore fibers are not involved in the formation of the first meiotic spindle in mouse oocytes, but control the exit from the first meiotic M phase. J Cell Biol 146:1–12.

Byskov AG, Andersen CY, Nordholm L, Thogersen H, Xia G, Wassmann O, Andersen JV, Guddal E, Roed T. 1995. Chemical structure of sterols that activate oocyte meiosis. Nature 374: 559–562.

Cha H, Wang X, Li H, Fornace AJ, Jr. 2007. A functional role for p38 MAPK in modulating mitotic transit in the absence of stress. J Biol Chem 282:22984–22992.

Choi JH, Adames NR, Chan TF, Zeng C, Cooper JA, Zheng XF. 2000. TOR signaling regulates microtubule structure and function. Curr Biol 10:861–864.

Choi JH, Bertram PG, Drenan R, Carvalho J, Zhou HH, Zheng XF. 2002. The FKBP12-rapamycin-associated protein (FRAP) is a CLIP-170 kinase. EMBO Rep 3:988–994.

Conti M, Hsieh M, Park JY, Su YQ. 2006. Role of the epidermal growth factor network in ovarian follicles. Mol Endocrinol 20: 715–723.

Cybulski N, Hall MN. 2009. TOR complex 2: A signaling pathway of its own. Trends Biochem Sci 34:620–627.

Delaval B, Letard S, Lelievre H, Chevrier V, Daviet L, Dubreuil P, Birnbaum D. 2005. Oncogenic tyrosine kinase of malignant hemopathy targets the centrosome. Cancer Res 65:7231–7240.

Doghman M, El-Wakil A, Cardinaud B, Thomas E, Wang J, Zhao W, Peralta-Del Valle MH, Figueiredo BC, Zambetti GP, Lalli E. 2010. Regulation of insulin-like growth factor-mammalian target of rapamycin signaling by microRNA in childhood adrenocortical tumors. Cancer Res 70:4666–4675.

Downs SM, Ya R, Davis CC. 2010. Role of AMPK throughout meiotic maturation in the mouse oocyte: Evidence for promotion of polar body formation and suppression of premature activation. Mol Reprod Dev 77:888–899.

Dujardin D, Wacker UI, Moreau A, Schroer TA, Rickard JE, De Mey JR. 1998. Evidence for a role of CLIP-170 in the establishment of metaphase chromosome alignment. J Cell Biol 141:849–862.

Dunlop EA, Tee AR. 2009. Mammalian target of rapamycin complex 1: Signalling inputs, substrates and feedback mechanisms. Cell Signal 21:827–835.